THE JOURNAL OF PHYSICAL CHEMISTRY C

ARTICLE

pubs.acs.org/JPCC

Co-Catalytic Solid-State Reduction Applied to Carbon Nanotube Growth

Bernhard C. Bayer,*[,†] Martin Fouquet,[†] Raoul Blume,[‡] Christoph T. Wirth,[†] Robert S. Weatherup,[†] Ken Ogata,[†] Axel Knop-Gericke,[§] Robert Schlögl,[§] Stephan Hofmann,[†] and John Robertson[†]

[†]Department of Engineering, University of Cambridge, Cambridge, CB3 0FA, United Kingdom

[‡]Helmholtz-Center Berlin for Materials and Energy, D-12487 Berlin, Germany

[§]Fritz-Haber-Institute of the Max-Planck-Society, D-14195 Berlin-Dahlem, Germany

Supporting Information

ABSTRACT: We report on a new class of cocatalysts for the chemical vapor deposition of carbon nanotubes, where the cocomponent (Ta) acts as a solid-state reducing agent for the active catalyst (Fe). The cocatalytic FeTa system enables carbon nanotube growth without the need for a reducing gas atmosphere such as H_2 or NH_3. In situ X-ray photoelectron spectroscopy reveals that the tantalum (oxide) getters the oxygen from the iron (oxide) by a diffusive solid-state process, driven by the much larger affinity to oxygen of Ta compared to Fe. We suggest that this redox-based mechanism is applicable to a wide range of metal (oxide)/catalyst systems and relevant to rational catalyst design in general heterogeneous catalysis.

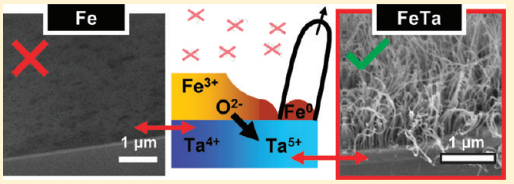

1. INTRODUCTION

The use of cocatalysts and multielemental catalyst composition to tune reactivity and selectivity is an approach well-known in heterogeneous catalysis.[1−5] Rational catalyst design, however, requires a detailed understanding of what causes the advantageous effect, and to date many of the actual mechanisms remain unknown. For the catalytic chemical vapor deposition (CVD) of carbon nanotubes (CNTs), single-element Fe, Co, and Ni remain the most commonly used catalyst materials,[6] but a number of bimetallic cocatalyst systems have been reported to enhance chiral selectivity, to narrow the diameter distribution, and to enhance yield and allow lower growth temperatures (e.g., CoMo,[7−12] FeRu,[13] NiFe,[14,15] CoMn,[16,17] CoCr,[18] FeCu,[19] CoW,[20,21] CoPd,[22] CoTi,[23] CoMn,[24] and FeMo[25−32]). However, the suggested cocatalytic interactions and mechansims are highly speculative and often rather contradictory in current literature. Here, we introduce a cocatalytic concept in carbon nanotube growth to add to the underdeveloped toolbox for rational catalyst design and provide experimental verification of the underlying atomic mechanism.

We have previously shown that the most common CNT catalyst material Fe is only active toward CNT growth in a reduced state[33] (where growth proceeds via either the metallic state or carbide formation[6,34]) but not as an oxide, when supported on common support materials such as SiO_2 and Al_2O_3.[33,35] However, the few-nanometer thin Fe catalyst films are usually oxidized during sample storage or transport in ambient air between catalyst preparation and CVD. Hence a reducing gas such as NH_3, H_2, hydrazine, or hot-filament cracked atomic H is necessary to activate the formed Fe oxide by reducing it back to Fe^0.[33,36,37] Here we show that with the admixture of tantalum to iron (FeTa) catalyst activation is achieved by solid-state reduction, where oxygen ions are transferred by diffusion from the oxidized Fe to the Ta. The thermodynamic driving force behind this is the much higher affinity to oxygen of the Ta compared to the Fe.[38,39] Fe-catalyzed CNT growth is thus achieved without the need for reducing gases, which was previously unattainable at similar pressures and temperatures (Figure 1).[33] This new approach enhances the degrees of freedom for CNT cocatalyst design and may be of use for various other catalytic processes.

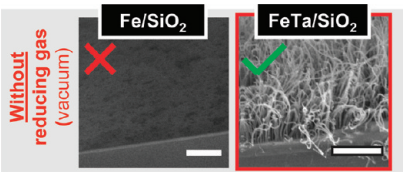

Figure 1. With the use of the FeTa cocatalyst we obtain Fe-catalyzed CNT carpet growth without the use of a reducing gas, i.e., in nonreducing conditions where growth from elemental Fe is unattainable (low-pressure CVD at ∼620 °C, vacuum pretreatment (45 min) followed by undiluted C_2H_2 growth (45 min), Fe 1 nm/Ta 2 nm. Scale bars = 1 μm.

2. EXPERIMENTAL DETAILS

We sputter deposit thin Ta layers (∼2 nm) onto SiO_2 covered Si wafers, followed by Fe catalyst layers (∼1 nm) where samples are exposed to ambient air in between depositions. As control samples, we deposit single-elemental Fe layers directly onto SiO_2

Received: October 21, 2011
Published: November 15, 2011

Table 1. Summary of Typical CVD Conditions

CVD conditions	base pressure	pretreatment (heat to ~620 °C, 5−45 min)	growth (at ~620 °C, 15−45 min)
low-pressure vacuum (was also used for in situ XPS)	$\sim 10^{-6}$ mbar	in 2×10^{-6} mbar vacuum	introduce C_2H_2 to 1×10^{-3} mbar
low-pressure Ar	$\sim 10^{-6}$ mbar	in 5×10^{-3} mbar Ar	add C_2H_2 to Ar to 6×10^{-3} mbar
low-pressure NH_3	$\sim 10^{-6}$ mbar	in 5×10^{-3} mbar NH_3	add C_2H_2 to NH_3 to 6×10^{-3} mbar
medium-pressure vacuum	$\sim 10^{-3}$ mbar	in 2×10^{-3} mbar vacuum	introduce C_2H_2 to 1×10^{-1} mbar
medium-pressure NH_3	$\sim 10^{-3}$ mbar	in 6×10^{-1} mbar NH_3	add C_2H_2 to NH_3 to 7×10^{-1} mbar

and similarly we deposit only single-elemental Ta layers onto SiO_2. Samples are then stored and transported in ambient air and these air exposed films are referred to as "as deposited" in this article. Film thicknesses are quoted with respect to the elemental metal thickness, but it should be noted that in ambient air the film thickness increases due to oxide formation. We estimate an experimental uncertainty in metal film thickness determination of ±30%.

Growth of CNTs from the FeTa/SiO_2, Fe/SiO_2, and Ta/SiO_2 samples is evaluated in a custom-built, cold-wall CVD system with the low- and medium-pressure CVD conditions as defined in Table 1. These conditions include both reducing (NH_3) and nonreducing pretreatment atmospheres (Ar and vacuum). A constant flux of C_2H_2 is added to the pretreatment atmosphere after a defined pretreatment time. The low-pressure CVD conditions provide little residual gas contamination and also allow the evolution of the surface chemistry to be measured by in situ X-ray photoelectron spectroscopy (XPS) at the ISISS end station of the FHI-MPG in the BESSY II synchrotron.[40] Samples are further characterized ex situ by scanning electron microscopy (SEM), scanning transmission electron microscopy (STEM) equipped with an energy dispersive X-ray spectrometer (EDX), and Raman spectroscopy. See Supporting Information for further details of experimental apparatus and methods.

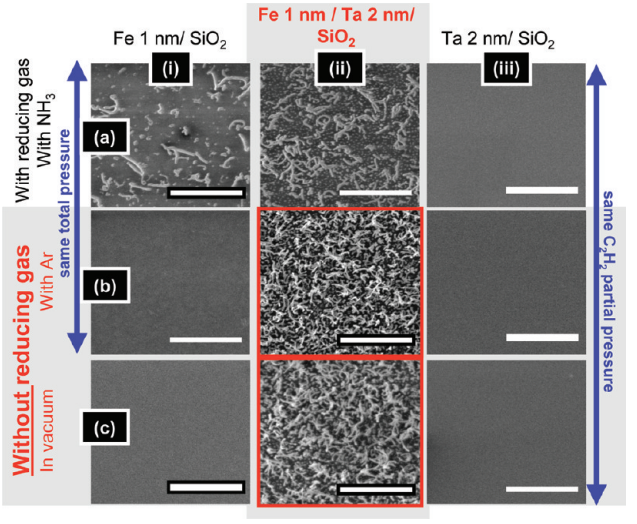

Figure 2. (a−c) Typical CNT growth results from low-pressure CVD at ~620 °C (5 min pretreatment and 15 min growth, see Table 1) with varying pretreatment conditions: (a) reducing with NH_3, (b) nonreducing with Ar, and (c) nonreducing in vacuum. During growth C_2H_2 is added to the pretreatment conditions. (i) Fe/SiO_2 control samples, (ii) FeTa cocatalyst. (iii) Pure Ta is inactive toward CNT growth under the low-pressure CVD conditions. Scale bars = 1 μm.

3. RESULTS

3.1. Ex Situ Growth Results. In Figure 2 the effects of varying the low-pressure CVD pretreatment atmosphere [rows (a−c)] on the different support/(co)catalyst systems [columns (i−iii)] are shown. The control experiment with pretreatment in a reducing gas [NH_3 (a), as in ref 33] is compared to pretreatment without a reducing gas [Ar (b) and vacuum (c)]. The partial C_2H_2 pressure is held constant for all three conditions, and for NH_3 and Ar the total pressure is also kept constant to exclude total pressure-related differences in pretreatment and growth.[41]

During low-pressure CVD with reducing NH_3 nanotubes nucleate on the Fe/SiO_2 as expected [Figure 2(a,i)]. The FeTa cocatalyst similarly nucleates CNTs when NH_3 is used [Figure 2(a,ii)]; however elemental Ta on SiO_2 does not [Figure 2(a,iii)]. The striking difference between the pristine Fe catalyst and the FeTa cocatalyst becomes evident when evaluating the CVD conditions *without* reducing NH_3 [parts b and c of Figure 2]: Fe/SiO_2 does not nucleate any CNTs without reducing NH_3, in agreement with ref 33. In clear contrast, the FeTa cocatalyst allows CNT nucleation without the reducing atmosphere. Both pretreatment in inert Ar [Figure 2(b,ii)] and in vacuum [Figure 2(c,ii)] result in CNT growth similar to the pretreatment in NH_3 [Figure 2(a,ii)]. Bare Ta layers [iii of parts b and c of Figure 2] without Fe again do not nucleate CNTs, confirming that bare Ta is catalytically inactive for CNT nucleation under the low-pressure CVD conditions. Additional STEM/EDX analysis of nanoparticles attached at the roots of nanotubes also shows that these particles are Fe and hence confirms that Fe is the nanotube nucleation catalyst while the Ta serves to activate the Fe (Figure S1 of the Supporting Information). Thus the *interplay* between Fe and Ta allows the CNT growth without the reducing pretreatment.

We exclude catalyst film thickness related effects by comparing the ~3 nm thick (sum of Ta and Fe thickness) cocatalyst layers also with single-elemental ~3 nm layers of Fe and Ta, respectively. These single-elemental layers show no growth under nonreducing conditions (not shown), ruling out that catalyst layer thickness-related effects might be responsible for the successful growth without a reducing gas.

The obtained CNTs are multiwalled with diameters of 5−45 nm, as evidenced by the STEM analysis in Figure 2 of Supporting Information. Catalyst particle diameters from samples which were only pretreated and the corresponding CNT diameters are in good agreement (Figure 2 of Supporting Information). The Raman spectra in Figure 3 of Supporting Information confirm that the CNTs from FeTa are of similar multiwalled-type and quality,[42] irrespective of whether a reducing gas is used or not. This implies that the addition of Ta to Fe influences the catalyst reduction/activation during pretreatment, rather than affecting the CNT nucleation.

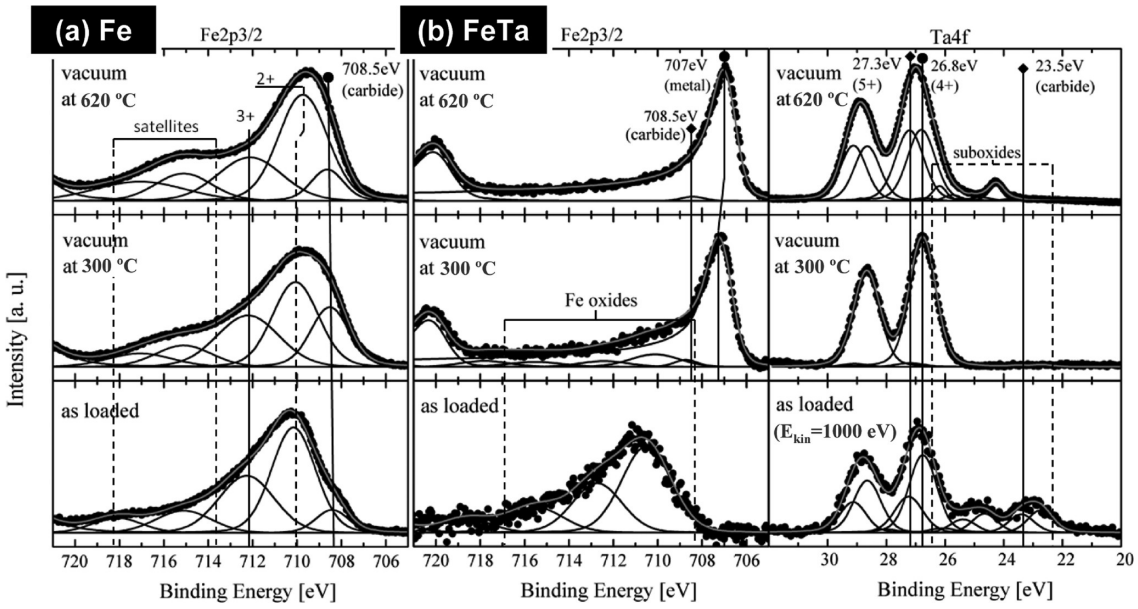

Figure 3. Process-step resolved in situ XP spectra of Fe/SiO_2 (a) and $FeTa/SiO_2$ (b) during vacuum-only pretreatment corresponding to Figure 2c. All spectra are recorded at a kinetic electron energy of 300 eV (corresponding to 0.9 nm information depth), apart from the lower right, as-loaded Ta4f, which was taken at 960 eV (1.5 nm), since the Ta was initially buried below the Fe film. Hence, the oxidation states in this scan are not directly comparable to the scans during vacuum heating above. Note that the small carbide peaks in the Fe2p and Ta4f are attributed to interactions with adventitious carbon from sample transport in ambient.

3.2. In Situ XPS Characterization. The ex situ growth results point to strongly enhanced reducibility of Fe oxide in the presence of Ta ("solid state reducing agent"), which activates the Fe catalyst even in nonreducing gas conditions. By using in situ XPS to directly measure the chemical interactions between the Fe and Ta during the CVD process,[39,40,43] we verify that FeTa allows instant Fe reduction under nonreducing conditions while Fe directly on SiO_2 stays oxidized.

Figure 3 shows process step resolved Fe2p and Ta4f core level XP spectra[33,35,44−48] during low-pressure CVD with pretreatment in vacuum only (followed by growth in pure C_2H_2, see Table 1, corresponding to Figure 2c). We compare Fe/SiO_2 control samples (Figure 3a) with $FeTa/SiO_2$ cocatalyst samples (Figure 3b). For the as-loaded samples we confirm that after transport in ambient air the pure Fe on the SiO_2 as well as the Fe and the Ta in the FeTa are oxidized. In the $Fe2p_{3/2}$ XP spectra we observe Fe^{2+} (709.7 eV) and Fe^{3+} (712.2 eV) and some satellites at higher binding energies. In the $Ta4f_{7/2}$ scans we find Ta^{4+} (26.8 eV), Ta^{5+} (27.3 eV), and a minor contribution of $Ta^{<4+}$ states (22−26 eV). (The as-loaded Ta4f scan was acquired at a higher kinetic electron energy compared to the scans at 300 and 620 °C. This was necessary since in the as deposited samples the Ta is buried by Fe. Thus, a different film depth is probed by XPS in the as loaded and the heated scans and therefore the oxidation states between those scans are not directly comparable. Additionally, a small carbidic component was found for Fe and Ta even without exposure to C_2H_2 which is attributed to interactions with adventitious carbon from sample transport in ambient.)

When heating the oxidized Fe on SiO_2 up to ∼620 °C in vacuum (for 45 min), the Fe remains oxidized. This lack of significant reduction is in agreement with our previous report in ref 33. Accordingly, no CNTs are grown from SiO_2/Fe with C_2H_2 exposure (45 min) following the vacuum pretreatment (Figure 1), corroborating the ex-situ growth results in Figure 2(c,i).

In contrast, the admixture of Ta to the Fe catalyst dramatically changes the chemical evolution under the same CVD conditions. In the presence of the Ta the Fe is already almost fully reduced (707.25 eV) by heating in vacuum to just ∼300 °C. At the growth temperature of ∼620 °C the Fe with Ta is fully reduced (707.05 eV). Corresponding to the reduction of the Fe during heating in vacuum, we find that also the oxidation state of the Ta changes. As noted above, the as-deposited Ta was not fully oxidized. At 300 °C, the surface sensitive Ta4f spectrum consists of mainly Ta^{4+} without any other suboxides, coinciding with the onset of reduction of Fe. At ∼620 °C, the oxidation state has shifted toward Ta^{5+}. Ta^{5+} and Ta^{4+} exhibit identical intensities, while simultaneously the Fe is completely reduced. (This is also reflected in the O1s XP scans in Figure 4 of Supporting Information. Additionally, a small Ta suboxide contribution emerges again which might point to structural rearrangement in the Ta oxide film.) We note that we do not observe XPS peak shifts associated with alloying of the Fe and the Ta,[44] as we did for metallic Fe and metallic Ta under similar conditions.[39] This indicates that the reduced Fe and the Ta oxide do not undergo intimate mixing. In agreement with full Fe oxide reduction, subsequent introduction of C_2H_2 to the FeTa cocatalyst sample yields homogeneous nanotube growth (Figure 1). In situ time-resolved monitoring of the C1s core level (Figure 5 of Supporting Information) confirms sp^2 carbon formation.[48]

The XPS measurements suggest an explanation for the observed beneficial cocatalytic interplay between Fe and Ta in Figure 2 on an atomistic level: When heating FeTa in a nonreducing atmosphere, the Fe oxide does not lose oxygen into the gas phase. Rather, oxygen ions from the Fe oxide are migrating to oxygen-deficient positions in the Ta oxide (thereby increasing its oxidation state toward Ta^{5+} with increased heating). Ta oxide with $Ta^{<5+}$ acts as an oxygen "sink" for the Fe oxide, thus reducing the Fe toward Fe^0. This process can proceed until either

dx.doi.org/10.1021/jp210137u |J. Phys. Chem. C 2012, 116, 1107–1113

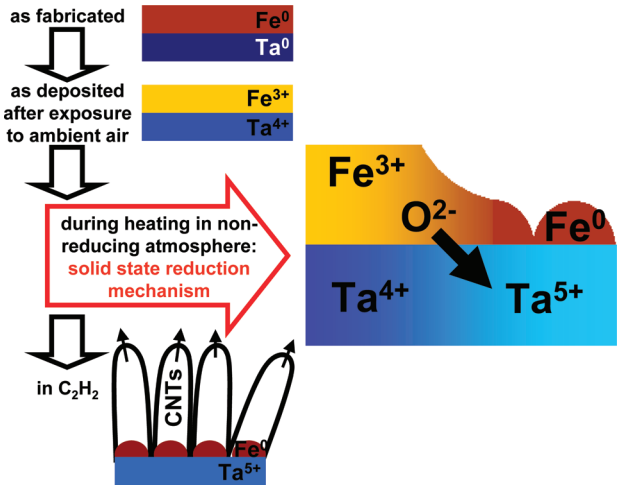

Figure 4. Schematic of solid-state reduction mechanism of Fe by Ta. $Ta^{<5+}$ oxides act as an oxygen "sink" for the Fe oxide: The oxides are initially formed after film deposition when the film is exposed to ambient air. This usually makes reduction of Fe by a reducing gas necessary to activate the catalyst. The addition of the Ta to the Fe lifts the necessity for this, since by oxygen transfer to the Ta, the Fe is reduced even in nonreducing atmospheres. The metallic Fe film then breaks into nanoparticles, which are active for CNT nucleation upon introduction of a carbon source gas.

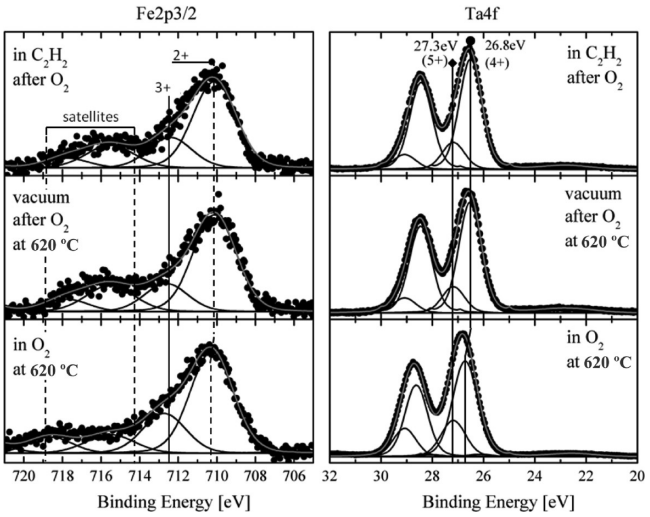

Figure 5. Process-step resolved in situ XPS spectra of $FeTa/SiO_2$ in the O_2 exposure cross-check (see text). When FeTa samples are exposed to pure O_2 (4×10^{-2} mbar) at ~620 °C both Fe and Ta are fully oxidized. Switching to vacuum after O_2 treatment does not lead to significant reduction of the Fe, unlike for as-deposited samples. We attribute this to complete filling of the oxygen "sink" in the Ta, hence deactivating the cocatalytic synergism. All spectra were recorded with photon energies corresponding to an electron kinetic energy of 300 eV and hence to an information depth of 0.9 nm.

the Fe is completely reduced or the Ta is fully oxidized. We find that with a film thickness ratio of Fe to Ta of 1:2 full reduction of the Fe can be achieved. The fully reduced Fe then nucleates CNTs on exposure to a carbon source gas without the need for a reducing gas. This mechanism is schematically summarized in Figure 4.

Since the Ta acts as a "sink" for the oxygen atoms from the Fe oxide, we conjecture that when the Ta is fully oxidized the solid-state reduction of the Fe should break down. We crosschecked this hypothesis by deliberately exposing a FeTa sample to 4×10^{-2} mbar O_2 at ~620 °C. As evidenced by the XPS measurements in Figure 5, this leads to full oxidation of the Ta (hence filling the "sink") as well as full oxidation of the Fe. The O_2 gas is then removed, returning to heating in vacuum as before. However, now under vacuum pretreatment the Fe remains in its oxidized form. The Ta, after heating in pure O_2, has no oxygen vacancies (or available oxidation states) to accommodate any additional oxygen atoms from the Fe oxide. In turn, this inhibits the cocatalytic synergetic reduction of the Fe into an active, metallic state just by heating in vacuum. Correspondingly, exposing such high temperature O_2 annealed samples to vacuum pretreatment, followed by C_2H_2 exposure, did not lead to any CNT growth (Figure 6 of Supporting Information).

Finally, we note that C_2H_2 is a mildly reducing gas itself, and indeed after growth times of >60 min we observe nucleation of sparse CNTs from SiO_2/Fe with pure C_2H_2 without an additional reducing gas. The CNT yield for this process is however greatly reduced (Figure 7 of Supporting Information) compared to the fast Ta-mediated growth (Figure 1).

4. DISCUSSION

We can estimate the necessary Fe:Ta material ratio to fully reduce a given amount of Fe oxide to Fe^0, based on our XPS observations. We simplify and assume that we shift all oxygen (by O^{2-} ion diffusion) from Fe^{3+} to the Ta by increasing the Ta oxidation state from Ta^{4+} to Ta^{5+} (Figure 4)

$$\begin{aligned} Fe^{3+} + 3e^- &\rightarrow Fe^0 \\ 3Ta^{4+} &\rightarrow 3Ta^{5+} + 3e^- \end{aligned} \quad (1)$$

This redox reaction implies a Fe to Ta ratio of 1:3 for the Fe to fully be reduced. This is close to our experimentally found optimal metal film thickness ratio of 1:2, especially considering the uncertainties in film thickness measurements (±30%) and the simplifying assumptions (only Fe^{3+} present, $Ta^{4+} \rightarrow Ta^{5+}$, neglecting suboxides). It also implies that when the Fe to Ta ratio is larger the solid-state reduction mechanism should break down, as there is not enough oxygen deficient Ta oxide to incorporate all the oxygen from the Fe oxide. We tested this by lowering the Ta thickness to ~0.5 nm (with constant Fe ~1 nm) and indeed found no growth without a reducing gas. Furthermore this reasoning also implies that for a smaller Fe to Ta ratio Fe oxide reduction still should be achieved. Hence, we also tested thicker Ta films (up to Ta ~100 nm) while keeping the Fe constant at ~1 nm. In this case, we indeed observe full reduction of Fe when heating without a reducing gas;[39] however, depletion of Fe by diffusion into the thick Ta oxide film (grain boundary diffusion) complicates the surface chemistry and leads to drastically reduced CNT growth. We have discussed Fe ~1 nm catalyst films on thick Ta films for CNT growth (for electrical interconnect applications) in ref 39.

We define a "solid-state reducing agent" as a material which by pure solid-state processes such as diffusion strips another, oxidized material of all oxygen. In the case of oxidized Fe for CNT growth this equates to catalyst activation. This is not to be confused with the well-known Fe-reduction promoters such as Cu, where Cu admixture to Fe is used to promote more efficient Fe oxide reduction *in a reducing gas*.[19,49] For our solid-state reducing agent mechanism no reducing gas is necessary.

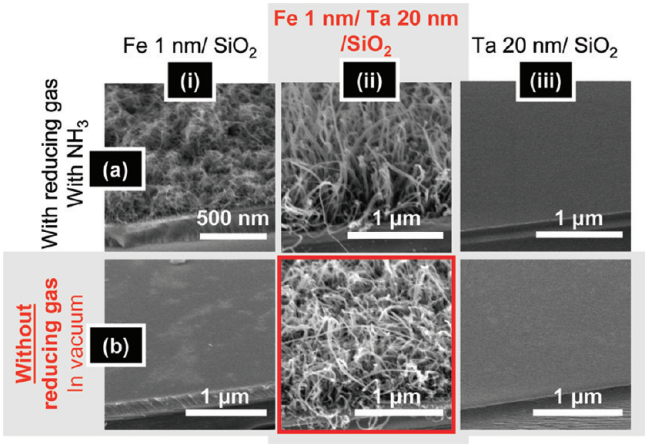

Figure 6. (a–b) Typical CNT growth results from medium-pressure CVD at ~620 °C (5 min pretreatment and 15 min growth, see Table 1) with varying pretreatment conditions: (a) reducing with NH_3 and (b) nonreducing in vacuum. During growth C_2H_2 is added to the pretreatment conditions. (i) Fe/SiO_2 control samples, (ii) FeTa cocatalyst. (iii) Pure Ta is inactive toward CNT growth under the medium-pressure CVD conditions. (SEM images tilted by ~60°.).

The thermodynamic driving force for the FeTa solid-state reduction mechanism is the difference in the affinities to oxygen of the two elements. Neglecting any kinetics, we can simplify and assume complete oxygen transfer from an initial Fe oxide to an initial Ta-metal in the thermite-like reaction

$$5Fe_2O_3 + 6Ta \rightarrow 3Ta_2O_5 + 10Fe \quad (2)$$

With the standard Gibbs free energies of formation of the oxide compounds (Fe_2O_3, −740 kJ/mol; Ta_2O_5, −1967 kJ/mol from ref 50) we estimate a standard Gibbs free energy of reaction of around −2000 kJ/mol for eq 2, indicating that the observed solid-state reduction is thermodynamically indeed favorable.[51] Note that accordingly, in the field of corrosion science, Fe cation reduction by oxidation of solid, metallic Ta was observed for Fe and O containing glass melts in contact with Ta sheets.[52] A wide range of further elements also show larger free energies of oxide-formation than Fe, including Zn, W, Mo, V, Cr, Nb, and Ti.[38] This suggests that some of these elements could show the same cocatalytic solid-state reduction effect. In fact, in ref 27 FeMo was shown to catalyze CNTs without a reducing gas in contrast to pristine Fe which needed activation by H_2. This was attributed to FeMo acting as an *oxide* catalyst, but no experimental characterization of the catalyst phase was made. In light of our findings, these results may reflect a solid-state Fe reduction by the Mo as well. Further studies are required to understand which element combinations can also act as solid-state reduction couples in cocatalysis.

A final corollary from our analysis is that the optimal Fe to Ta ratio should depend on the initial degree of oxidation of the films. A higher residual oxygen (or water) contamination, as found in a system with an inferior base pressure compared to the low-pressure conditions, will fill up some of the Ta's reservoir for oxygen, and hence more Ta will then be required for the same effect of solid-state reduction and catalyst activation for a constant amount of Fe. We tested this by growing CNTs from FeTa samples under medium-pressure CVD conditions with a ~1000-times worse base pressure compared to low-pressure CVD (Table 1). In complete agreement with the low-pressure results (Figure 2), we find growth under nonreducing conditions for FeTa but not for pure Fe (and pure Ta) in medium-pressure CVD (Figure 6). However, testing various thicknesses of Ta from 0.5 to 100 nm (with Fe fixed at 1 nm), we note that the necessary Fe to Ta ratio to see catalyst activation has shifted from 1:2 for low-pressure to 1:20 for medium-pressure CVD. This is due to the higher levels of initial Ta oxidation from the less clean residual gas background in medium-pressure, as inferred above. In addition, and in agreement with generally increased CNT growth rates with increasing carbon source partial pressure,[53] the CNT yield was significantly increased for the medium-pressure CVD (at constant process times). This implies further scalability of solid-state reduction cocatalytic CNT growth based on our elucidation of the atomic mechanism.

Our findings add to the toolbox of rational CNT catalyst design but are not limited to this: Cocatalytic effects like in the FeTa system also need to be considered for high yield CNT forest growth on functional support materials. In this case, at the interface between the support and the catalyst, similar redox reactions can influence the state of the catalyst and thus CNT nucleation.[39,54−57] Furthermore, besides lifting the requirement to use a reducing gas for CNT CVD which can have economic or environmental benefits, our findings also imply some application perspective for Fe-catalyzed CNT growth on substrates where strongly reducing atmospheres are detrimental to substrate stability, for example, on certain oxides such as LSMO which is used for spintronics. Beyond CNT growth, the solid-state reducing mechanism is of interest for closely related catalytic processes such as nonoxidative catalytic dehydrogenation of hydrocarbon gases for production of carbon-oxide-free hydrogen gas.[58,59] There it was recently shown that bimetallic catalysts that ease Fe reduction increase reaction activity.[60,61] More generally, the comparably easy reduction and activation of Fe in the presence of Ta at temperatures as low as 300 °C and without the need for reducing gases may also find interest in other fields of catalysis, for example, for initial catalyst activation in the economically highly important Fischer–Tropsch synthesis.

5. CONCLUSIONS

In conclusion, we present evidence for a new class of cocatalysts in CNT CVD, where one component acts as a solid-state reducing agent for the other component. In particular, the addition of Ta allows Fe-catalyzed growth of CNTs without the need for a reducing gas because the Ta acts as a nanoscale oxygen getter for the Fe (oxide). This mechanism adds to rational catalyst design of cocatalysts in CNT CVD. Beyond cocatalytic CNT growth, our findings may generally benefit catalytic processes which require reduced Fe at low temperatures and/or do not allow strongly reducing atmospheres.

■ ASSOCIATED CONTENT

Supporting Information. More details on apparatus and methods. Additional STEM, SEM, Raman, and XPS data. This material is available free of charge via the Internet at http://pubs.acs.org.

■ AUTHOR INFORMATION

Corresponding Author

*Phone: +44/1223/748377. Fax: +44/1223/748348. E-mail: bcb25@cam.ac.uk.

■ ACKNOWLEDGMENT

We acknowledge funding from the EU Integrated Project "Technotubes" under Grant No. 226716. We acknowledge the Helmholtz−Zentrum−Berlin BESSY II synchrotron, and we thank the BESSY staff for continuous support. S.H. acknowledges funding from EPSRC (Grant No. EP/H047565/1). R.S.W. acknowledges funding from the EPSRC (Doctoral training award).

■ REFERENCES

(1) Sinfelt, J. H. *Acc. Chem. Res.* **1977**, *10*, 15–20.
(2) Toshima, N.; Yonezawa, T. *New J. Chem.* **1998**, *22*, 1179–1201.
(3) Thomas, J. H.; Johnson, B. F. G.; Raja, R.; Sankar, G.; Midgley, P. A. *Acc. Chem. Res.* **2003**, *36*, 20–30.
(4) Fernandez, J. L.; Walsh, D. A.; Bard, A. J. *J. Am. Chem. Soc.* **2005**, *127*, 357–365.
(5) Stamenkovic, V. R.; Mun, B. S.; Arenz, M.; Mayrhofer, K. J. J.; Lucas, C. A.; Wang, G.; Ross, P. N.; Markovic, N. M. *Nat. Mater.* **2007**, *6*, 241–247.
(6) Tessonnier, J.-P.; Su, D. S. *ChemSusChem* **2011**, *4*, 824–847.
(7) Kitiyanan, B.; Alvarez, W. E.; Harwell, J. H.; Resasco, D. E. *Chem. Phys. Lett.* **2000**, *317*, 497–503.
(8) Bachilo, S. M.; Balzano, L.; Herrera, J. E.; Pompeo, F.; Resasco, D. E.; Weisman, R. B. *J. Am. Chem. Soc.* **2003**, *125*, 11186–11187.
(9) Herrera, J. E.; Balzano, L.; Borgna, A.; Alvarez, W. E.; Resasco, D. E. *J. Catal.* **2001**, *204*, 129–145.
(10) Herrera, J. E.; Resasco, D. E. *J. Catal.* **2004**, *221*, 354–364.
(11) Lolli, G.; Zhang, L.; Balzano, L.; Sakulchaicharoen, N.; Tan, Y.; Resasco, D. E. *J. Phys. Chem. B.* **2006**, *110*, 2108–2115.
(12) Wang, B.; Poa, C. H. P.; Wei, L.; Li, L.; Yang, Y.; Chen, Y. *J. Am. Chem. Soc.* **2007**, *129*, 9014–9019.
(13) Li, X.; Tu, X.; Zaric, S.; Welsher, K.; Seo, W. S.; Zhao, W.; Dai, H. *J. Am. Chem. Soc.* **2007**, *129*, 15770–15771.
(14) Chiang, W.; Sankaran, R. M. *Nat. Mater.* **2009**, *8*, 882–886.
(15) Chiang, W.; Sankaran, R. M. *Adv. Mater.* **2008**, *20*, 4857–4861.
(16) Loebick, C. Z.; Podila, R.; Reppert, J.; Chudow, J.; Ren, F.; Haller, G. L.; Rao, A. M.; Pfefferle, L. D. *J. Am. Chem. Soc.* **2010**, *132*, 11125–11131.
(17) Loebick, C. Z.; Derrouiche, S.; Marinkovic, N.; Wang, C.; Hennrich, F.; Kappes, M. M.; Haller, G. L.; Pfefferle, L. D. *J. Phys. Chem. C* **2009**, *113*, 21611–21620.
(18) Loebick, C. Z.; Derrouiche, S.; Fang, F.; Li, N.; Haller, G. L.; Pfefferle, L. D. *Appl. Catal., A* **2009**, *368*, 40–49.
(19) He, M.; Chernov, A. I.; Fedotov, P. V.; Obraztsova, E. D.; Sainio, J.; Rikkinen, E.; Jiang, H.; Zhu, Z.; Tian, Y.; Kauppinen, E. I.; Niemela, M.; Krause, A. O. I. *J. Am. Chem. Soc.* **2010**, *132*, 13994–13996.
(20) Herrera, J. E.; Resasco, D. E. *J. Phys. Chem. B* **2003**, *107*, 3738–3746.
(21) Landois, P.; Peigney, A.; Laurent, C.; Frin, L.; Datas, L.; Flahaut, E. *Carbon* **2009**, *47*, 789–794.
(22) Berenguer, A.; Cantoro, M.; Golovko, V. B.; Hofmann, S.; Wirth, C. T.; Johnson, B. F. G.; Robertson, J. *Phys. Status Solidi B* **2009**, *11−12*, 2436–2439.
(23) Sato, S.; Kawabata, A.; Kondo, D.; Nihei, M.; Awano, Y. *Chem. Phys. Lett.* **2005**, *402*, 149–154.
(24) Tessonnier, J.-P.; Becker, M.; Xia, W.; Girgsdies, F.; Blume, R.; Yao, L.; Su, D. S.; Muhler, M.; Schlögl, R. *ChemCatChem* **2010**, *2*, 1559–1561.
(25) Yoshida, H.; Shimizu, T.; Uchiyama, T.; Kohno, H.; Homma, Y.; Takeda, S. *Nano Lett.* **2009**, *9*, 3810–3815.
(26) Christen, H. M.; Puretzky, A. A.; Cui, H.; Belay, K.; Fleming, P. H.; Geohegan, D. B.; Lowndes, D. H. *Nano Lett.* **2004**, *4*, 1939–1942.
(27) Harutyunyan, A. R.; Pradhan, B. K.; Kim, U. J.; Chen, G.; Eklund, P. C. *Nano Lett.* **2002**, *2*, 525–530.
(28) Harutyunyan, A. R.; Mora, E.; Tokune, T.; Bolton, K.; Rosen, A.; Jiang, A.; Awasthi, N.; Curtarolo, S. *Appl. Phys. Lett.* **2007**, *90*, 163120−1–163120−3.
(29) Pint, C. L.; Nicholas, N.; Pheasant, S. T.; Duque, J. G.; Parra-Vasquez, A. N. G.; Eres, G.; Pasquali, M.; Hauge, R. H. *J. Phys. Chem. C.* **2008**, *112*, 14041–14051.
(30) Cordier, A.; de Resende, V. G.; De Grave, E.; Peigney, A.; Laurent, C. *J. Phys. Chem. C* **2008**, *112*, 18825–18831.
(31) Lamouroux, E.; Serp, P.; Kihn, Y.; Kalck, P. *Catal. Commun.* **2006**, *7*, 604–609.
(32) Lamouroux, E.; Serp, P.; Kihn, Y.; Kalck, P. *Appl. Catal., A* **2007**, *323*, 162–173.
(33) Hofmann, S.; Blume, R.; Wirth, C. T.; Cantoro, M.; Sharma, R.; Ducati, C.; Hävecker, M.; Zafeiratos, S.; Schnoerch, P.; Oesterreich, A.; Teschner, D.; Albrecht, M.; Knop-Gericke, A.; Schlögl, R.; Robertson, J. *J. Phys. Chem. C* **2009**, *113*, 1648–1656.
(34) Nishimura, K.; Okazaki, N.; Pan, L.; Nakayama, Y. *Jpn. J. Appl. Phys.* **2004**, *43*, L471–L474.
(35) Mattevi, C.; Wirth, C. T.; Hofmann, S.; Blume, R.; Cantoro, M.; Ducati, C.; Cepek, C.; Knop-Gericke, A.; Milne, S.; Castellarin-Cudia, C.; Dolafi, S.; Goldoni, A.; Schloegl, R.; Robertson, J. *J. Phys. Chem. C* **2008**, *112*, 12207–12213.
(36) Pint, C. L.; Kim, S. M.; Stach, E. A.; Hauge, R. H. *ACS Nano* **2009**, *3*, 1897–1905.
(37) Pint, C. L.; Pheasant, S. T.; Parra-Vasquez, A. N. G.; Horton, C.; Xu, Y.; Hauge, R. H. *J. Phys. Chem. C* **2009**, *113*, 4125–4133.
(38) Robertson, J.; Sharia, O.; Demkov, A. A. *Appl. Phys. Lett.* **2007**, *91*, 132912−1–132912−3.
(39) Bayer, B. C.; Hofmann, S.; Castellarin-Cudia, C.; Blume, R.; Baehtz, C.; Esconjauregui, S.; Wirth, C. T.; Oliver, R. A.; Ducati, C.; Knop-Gericke, A.; Schlögl, R.; Goldoni, A.; Cepek, C.; Robertson, J. *J. Phys. Chem. C* **2011**, *115*, 4359–4369.
(40) Knop-Gericke, A.; Kleimenov, E.; Hävecker, M.; Blume, R.; Teschner, D.; Zafeiratos, S.; Schlögl, R.; Bukhtiyarov, V. I.; Kaichev, V. V.; Prosvirin, I. P.; Nizovskii, A. I.; Bluhm, H.; Barinov, A.; Dudin, P.; Kiskinova, M. *Adv. Catal.* **2009**, *52*, 213–272.
(41) Pisana, S.; Cantoro, M.; Parvez, A.; Hofmann, S.; Ferrari, A. C.; Robertson, J. *Physica E* **2007**, *37*, 1–5.
(42) Jorio, A.; Pimenta, M. A.; Souza Filho, A. G.; Saito, R.; Dresselhaus, G.; Dresselhaus, M S. *New J. Phys.* **2003**, *5*, 139.1–139.17.
(43) Steiner, S. A., III; Baumann, T. F.; Bayer, B. C.; Blume, R.; Worsley, M. A.; MoberlyChan, W. J.; Shaw, E. L.; Schlögl, R.; Hart, A. J.; Hofmann, S.; Wardle, B. L. *J. Am. Chem. Soc.* **2009**, *131*, 12144–12154.
(44) Yang, D.; Jiang, H.; Ott, R.; Minor, K.; Grant, J.; Varga, L.; Barnard, J. A.; Doyle, W. D. *Surf. Interface Anal.* **1999**, *27*, 259–272.
(45) Khanuja, M.; Sharma, H.; Mehta, B. R.; Shivaprasad, S. M. J. Electron Spectrosc. Relat. Phenom. **2009**, *169*, 41–45.
(46) Atanassova, E.; Tyuliev, G.; Paskaleva, A.; Spassov, D.; Kostov, K. *Appl. Surf. Sci.* **2004**, *225*, 86–99.
(47) Itchkawitz, B. S.; Lyman, P. F.; Ownby, G. W.; Zehner, D. M. *Surf. Sci.* **1994**, *318*, 395–402.
(48) Hofmann, S.; Sharma, R.; Ducati, C.; Du, G.; Mattevi, C.; Cepek, C.; Cantoro, M.; Pisana, S.; Parvez, A.; Cervantes-Sodi, F.; Ferrari, A. C.; Dunin-Borkowski, R.; Lizzit, S.; Petaccia, L.; Goldoni, A.; Robertson, J. *Nano Lett.* **2007**, *7*, 602–608.
(49) de Smit, E.; de Groot, F. M. F.; Blume, R.; Hävecker, M.; Knop-Gericke, A.; Weckhuysen, B. M. *Phys. Chem. Chem. Phys.* **2010**, *12*, 667–680.
(50) Weast, R. C. *CRC Handbook of Chemisty and Physics*; CRC Press: Cleveland, 1975; pp D-67−D-77.
(51) Kubaschewski, O.; Alcock, C. B. *Metallurgical Thermochemistry*; Pergamon Press: Oxford, 1979.
(52) Podor, R.; Rapin, C.; David, N.; Mathieu, S. *J. Electrochem. Soc.* **2004**, *151*, B661–B668.
(53) Wirth, C. T.; Zhang, C.; Zhong, G.; Hofmann, S.; Robertson, J. *ACS Nano* **2009**, *3*, 3560–3566.
(54) Esconjauregui, S.; Bayer, B. C.; Fouquet, M; Wirth, C. T.; Yan, F.; Xie, R.; Ducati, C.; Baehtz, C.; Castellarin-Cudia, C.; Bhardwaj, S.; Cepek, C.; Hofmann, S.; Robertson, J. *J. Appl. Phys.* **2011**, *109*, 114312−1–114312−10.
(55) Wang, Y.; Luo, Z.; Li, B.; Ho, P. S.; Yao, Z.; Shi, L.; Bryan, E. N.; Nemanich, R. J. *J. Appl. Phys.* **2007**, *101*, 124310−1–124310−8.

(56) Nessim, G. D.; Seita, M.; O'Brien, K. P.; Hart, A. J.; Bonaparte, R. K.; Mitchell, R. R.; Thompson, C. V. *Nano Lett.* **2009**, *9*, 3398–3405.
(57) Bayer, B. C.; Zhang, C.; Blume, R.; Yan, F.; Fouquet, M.; Wirth, C. T.; Weatherup, R. S.; Lin, L.; Baehtz, C.; Oliver, R. A.; Knop-Gericke, A.; Schlögl, R.; Hofmann, S.; Robertson, J. *J. Appl. Phys.* **2011**, *109*, 114314−1–114314−7.
(58) Shah, N.; Panjala, D.; Huffman, G. P. *Energ. Fuel* **2001**, *15*, 1528–1534.
(59) Shah, N.; Wang, Y.; Panjala, D.; Huffman, G. P. *Energ. Fuel* **2004**, *18*, 727–735.
(60) Punnoose, A.; Shah, N.; Huffman, G. P.; Seehra, M. S. *Fuel Process. Technol.* **2003**, *83*, 263–273.
(61) Shah, N.; Pattanaik, S.; Huggins, F. E.; Panjala, D.; Huffman, G. P. *Fuel Process. Technol.* **2003**, *83*, 163–173.